Time-delayed probe spectroscopy in two-photon—pumped systems

A. Guzman de Garcia and P. Meystre
Max-Planck-Institut für Quantenoptik, D-8046 Garching bei München, Federal Republic of Germany

R. R. E. Salomaa
Department of Technical Physics, Helsinki University of Technology, SF-02150 Espoo 15, Finland
(Received 16 April 1985)

We study transients in resonantly coupled three-level systems. Two of the levels are coupled by intense two-photon pumping, and the third one provides a probing level. Adiabatically eliminated levels appear in effective system parameters. Experimentally, this model is applicable, e.g., in resonantly enhanced parametric and harmonic generation in atomic vapors. A distinguishing feature in the system is the appearance of ac Stark shifts in the probe spectra when pumping at the two-photon resonance. The nutation signal is shown to give information on the effective two-photon Rabi frequency and on the decay rate of the dipole-forbidden two-photon coherence. Free-induction decay is strongly dominated by population-induced effects; Raman-like peaks introduced by Stark shifts may show large instantaneous gain. Gaussian pump pulses are investigated to investigate effects arising from the temporal sweeping of the two-photon Rabi flipping and the modulation of the Stark shifts. The results also provide relevant information on the gain dynamics of coherently pumped lasers.

I. INTRODUCTION

The study of transients in three-level systems has been the object of considerable work (see, e.g., Refs. 1—12) dealing in particular with effects such as optical nutation[5] and free-induction decay,[6—8] as well as with more elaborate techniques including photon echoes,[5,6,9,10] delayed-pulse spectroscopy,[6] self-induced transparency,[11] two-pulse delayed spectroscopy,[6] etc. The measurement of transients provides information on atomic and molecular systems complementary to that given by the methods of saturation spectroscopy. While those yield information in the frequency domain, transient effects give directly the time domain dynamics of the system, and as such constitute a powerful tool to measure relaxation rates.

It is natural to search for spectroscopic techniques that combine the advantages of both, i.e., that deliver simultaneously time- and frequency-domain information. Ducloy *et al.*[1] have proposed such a technique. It consists of applying a weak probe field to the system and monitoring its gain profile at various times, or equivalently in measuring transients at various probe frequencies.

In this paper, we apply a similar technique to study the dynamical behavior of two-photon pumped atomic systems. Specifically, we consider a two-photon pumped three-level system (see Fig. 1), which differs from the usual (one-photon pumped) case in that all transitions are now allowed, one of them being the two-photon transition $|1\rangle$-$|2\rangle$. We show that its transient response yields information about relaxation rates, and in particular about the two-photon coherence relaxation rate γ_{12}, not available from standard linewidth measurements.

The appearance of two-photon dynamic Stark shifts, which act even at the two-photon resonance as intensity-dependent detunings, leads to further distinctions between this and the standard three-level system. The onset and disappearance of these shifts following a sudden switch on or off of a strong pump field E_1 can be monitored by measuring the gain profile of a weak probe field E_2 nearly resonant with the $|2\rangle$-$|3\rangle$ transition. Finally, the transient behavior allows a clear distinction to be made between Raman-type and population-type contributions to the dynamics of the system.

The remainder of this paper is organized as follows. In Sec. II, we introduce our model and develop the density matrix equations of the system, introducing the effective two-photon matrix element and the two-photon Stark shifts. This formalism is then used in Sec. III to discuss the optical nutation effects occuring after sudden switch on of the pump field E_1. Free-induction decay is analyzed in Sec. IV for the case where the system has reached steady state before E_1 is switched off. In both Secs. III and IV, square pump pulses are considered. This restriction is removed in Sec. V, where Gaussian pump pulses are introduced. Finally, Sec. VI contains a summary and conclusions.

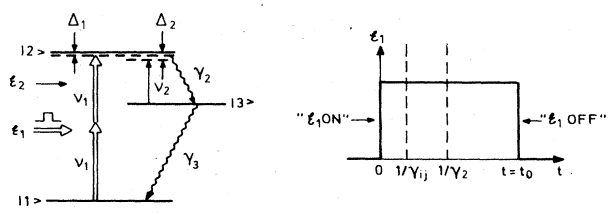

FIG. 1. Level scheme with the weak cw probe field E_2 at frequency ν_2 coupling to the $|2\rangle$-$|3\rangle$ transition and the pump beam E_1 at frequency ν_1 coupling levels $|1\rangle$ and $|2\rangle$.

A major flaw of pump-probe techniques, when applied to complicated systems, is that the results typically depend on a considerable number of parameters. In order to simplify the analysis of the data, it is crucial, both experimentally and theoretically, to consider limiting cases where at least some of these parameters can be eliminated. General solutions are in fact quite complicated and useless, and we therefore limit our discussion to some illustrative limiting cases.

Finally, it should be noted that a further generalization of the system discussed here would include the use of two probe beams, one of them about the $|2\rangle$-$|3\rangle$ and the other about the $|3\rangle$-$|1\rangle$ transition. This gives rise to parametric and four-wave-mixing transients—an interesting subject worth more extensive explorations in the future.

II. THEORETICAL FORMALISM

Two-photon resonant transitions are second-order processes which take place through intermediate nonresonant dipole allowed transitions.[13] For strong pump fields, considerable population can be transferred into the upper resonant state so that a nonperturbative description of the dynamics of the system is required.

To rigorously take into account all intermediate levels poses insurmountable difficulties, but if all of them are strongly detuned, their probability amplitudes are calculable by perturbation theory. Furthermore, the large detunings enable the intermediate levels to adiabatically follow the switching on and off of the fields. (Note the limitations on pulse rise and fall times imposed by this assumption.) In this situation, the dynamics of the system is satisfactorily described by a simple two-photon, two-level Bloch model[4,14] in which the intermediate levels are eliminated and their influence included into an effective Rabi frequency and into Stark shifts of the resonant levels. The original two-level model is easily modified to include a third, near-resonant level (see Fig. 1). In this case, the electromagnetic field is described by the electric field

$$E(t)=[\tfrac{1}{2}E_1(t)\exp(-i\nu_1 t)+\tfrac{1}{2}E_2(t)\exp(-i\nu_2 t)]+\text{c.c.}\ , \tag{1}$$

where E_1 and E_2 are slowly varying field amplitudes including the spatial variation and ν_1 and ν_2 are the pump and probe frequencies, respectively. In a previous paper,[15] we expanded the relevant elements of the atomic density matrix in the Fourier series and obtained equations for the resonant, slowly varying components by adiabatic elimination of the nonresonant ones. We neglected the contributions of nonresonant polarizations between intermediate states, which lead to the introduction of a partial two-photon matrix element V_{12R} in the equations of motion. More recently, we applied the same method,[16] but considering all nonresonant components exactly to first order in the fields.[17] We obtained then equations similar to those of an ordinary three-level system, recovering the total two-photon matrix element V_{12} everywhere in the equations of motion, namely

$$\begin{aligned}
\frac{d\rho_{21}}{dt}&=-(\gamma_{21}+i\Delta_1+i\omega_{s1}I_1)\rho_{21}\\
&\quad -iV_{23}\rho_{31}+iV_{21}(\rho_{22}-\rho_{11})\ ,\\
\frac{d\rho_{23}}{dt}&=-(\gamma_{23}+i\Delta_2+i\omega_{s2}I_1)\rho_{23}\\
&\quad -iV_{21}\rho_{13}+iV_{23}(\rho_{22}-\rho_{33})\ ,\\
\frac{d\rho_{13}}{dt}&=-(\gamma_{13}-i\Delta_3-i\omega_{s3}I_1)\rho_{13}+iV_{23}\rho_{12}-iV_{12}\rho_{23}\ ,\\
\frac{d\rho_{11}}{dt}&=\gamma_3\rho_{33}+(iV_{21}\rho_{12}+\text{c.c.})\ ,\\
\frac{d\rho_{22}}{dt}&=-\gamma_2\rho_{22}-[(iV_{21}\rho_{12}+iV_{23}\rho_{32})+\text{c.c.}]\ ,\\
\frac{d\rho_{33}}{dt}&=-\gamma_3\rho_{33}+\gamma_2\rho_{22}+(iV_{23}\rho_{32}+\text{c.c.})\ .
\end{aligned} \tag{2}$$

Here, γ_j is the decay constant of level $|j\rangle$ and γ_{ij} the relaxation rate of the coherence ρ_{ij}, ω_{ij} are the atomic transition frequencies, $\Delta_1=\omega_{21}-2\nu_1$ and $\Delta_2=\omega_{23}-\nu_2$ are the pump and probe detunings, respectively, and $\Delta_3=\Delta_1-\Delta_2$. Doppler shifts are easily included in the detunings in the case of traveling waves, but we shall ignore them here. The reduced interaction matrix elements V_{ij} are given by

$$\begin{aligned}
V_{23}&=-\frac{d_{23}E_2}{2\hbar}\ ,\\
V_{21}&=\frac{k_{21}E_1^2}{2\hbar}\ ,
\end{aligned} \tag{3}$$

where d_{ij} is the electric dipole matrix element for the $|i\rangle$-$|j\rangle$ transition, and k_{21} is the effective two-photon coupling constant

$$k_{21}=\frac{1}{2\hbar}\sum_j\frac{d_{2j}d_{j1}}{\omega_{2j}-\nu_1}\ . \tag{4}$$

The two-photon ac Stark shifts $\omega_{si}I_1$, $i=1,2,3$, have been expressed in terms of the dimensionless pump intensity $I_1=2|V_{21}|\sqrt{T_1/\gamma_{21}}$, with

$$T_1=\tfrac{1}{2}(2/\gamma_2+1/\gamma_3)$$

and

$$\begin{aligned}
\omega_{s1}&=-\frac{1}{2\hbar}\sum_j\left[\frac{|d_{ij}|^2\omega_{1j}}{\omega_{ij}^2-\nu_1^2}+\frac{|d_{2j}|^2\omega_{j2}}{\omega_{j2}^2-\nu_1^2}\right]\\
&\quad\times(1/k_{21}\sqrt{T_1/\gamma_{21}})\ ,\\
\omega_{s2}&=-\frac{1}{2\hbar}\sum_j\left[\frac{|d_{3j}|^2\omega_{3j}}{\omega_{3j}^2-\nu_1^2}+\frac{|d_{j2}|^2\omega_{j2}}{\omega j_2^2-\nu_1^2}\right]\\
&\quad\times(1/k_{21}\sqrt{T_1/\gamma_{21}})\ ,\\
\omega_{s3}&=\omega_{s1}-\omega_{s2}\ .
\end{aligned} \tag{5}$$

The detailed analytical procedure to obtain Eqs. (2) is given in Ref. 16. The main assumptions and requirements involved are the following: (1) the adiabatic criterion $|dE_1/dt| \ll |\Delta_{lj}E_1|$ must be satisfied for each intermediate detuning Δ_{lj}, i.e., the pump field should be adiabatically applied with respect to all intermediate states, but not necessarily with respect to the resonant levels; (2) the coupling between nonresonant amplitudes is neglected; (3) only first order terms in the probe field are kept; (4) the resonant states under consideration are nondegenerate.

In this paper, we assume a thin sample in which the fields radiated by the medium remain small compared to the external fields and where pump depletion due to two-photon absorption is negligible. The requirement for the probe gain g is that $gL \ll 1$, where g is proportional to $\mathrm{Im}(\rho_{23})$ and L is the sample length. The condition $gL \ll 1$ also implies that the output field is simply given by

$$E(L,t)=E(0,t-L/v)(1+gL)\ , \tag{6}$$

where v is the speed of light in the medium. Having optically thin samples avoids complications due to propagation and phase-matching effects and thus benefits from an easier analysis of the data.

An analytical expression for the small signal gain is obtained by solving the density matrix equations (2) to first order in the probe field. The zeroth-order solution in V_{23} obeys the equations

$$\begin{aligned}
&\frac{d\rho_{11}^0}{dt}=\gamma_3\rho_{33}^0+(iV_{21}\rho_{12}^0+\text{c.c.})\ ,\\
&\frac{d\rho_{22}^0}{dt}=-\gamma_2\rho_{22}^0-(iV_{21}\rho_{12}^0+\text{c.c.})\ ,\\
&\frac{d\rho_{33}^0}{dt}=\gamma_2\rho_{22}^0-\gamma_3\rho_{33}^0\ ,\\
&\frac{d\rho_{21}^0}{dt}=-(\gamma_{21}+i\Delta_1')\rho_{21}^0+iV_{21}(\rho_{22}^0-\rho_{11}^0)\ ,\\
&\rho_{13}^0=0\ ,\\
&\rho_{23}^0=0\ .
\end{aligned} \tag{7}$$

After solving these we obtain the coherences ρ_{23}^1 and ρ_{13}^1 from

$$\begin{aligned}
&\frac{d\rho_{23}^1}{dt}=-(\gamma_{23}+i\Delta_2')\rho_{23}^1+iV_{23}(\rho_{22}^0-\rho_{33}^0)-iV_{21}\rho_{13}^1\ ,\\
&\frac{d\rho_{13}^1}{dt}=-(\gamma_{13}-i\Delta_3')\rho_{13}^1+iV_{23}\rho_{12}^0=iV_{12}\rho_{23}^1\ .
\end{aligned} \tag{8}$$

The superscript denotes the order of perturbation in V_{23}. We have also introduced the intensity-dependent detuning $\Delta_i'=\Delta_i+\omega_{si}I_1$.

In the following, we shall assume that $\gamma_3 \gg \gamma_2$. This is not a necessary requirement, but reduces the number of equations because the population accumulation onto level $|3\rangle$ remains negligible, leading to some simplification of the analytical calculations.

For square pump pulses, analytical solutions of Eqs. (7) and (8) are easily found by the Laplace transform. But the general expressions are rather complicated and lack transparency. We shall therefore consider here only some illustrative limiting cases which most easily reveal the underlaying main physical features and which also allow the most reliable extraction of spectroscopic parameters from experimental data. As regards the pulse shapes, it is worth recalling once more that our transient analysis is valid only for "adiabatic square pulses," i.e., pulses which rise and fall in a time short compared with any relaxation time of the system of resonant levels, but still long enough to satisfy the adiabatic criterion with respect to the intermediate transitions.

III. OPTICAL NUTATION

We consider first the situation where the atomic system is initially in its ground state, i.e., $\rho_{ij}(0)=\delta_{1i}\delta_{1j}$, with a weak cw probe E_2 applied to it (see Fig. 1). The strong field E_1 is switched on at the time $t=0$. The transient response of the system, usually called optical nutation, is monitored by measuring the time-dependent gain spectrum of E_2. In steady state,[15] the gain spectrum consists of two peaks due to the dynamic Stark splitting of the upper level. A pecularity of two-photon pumped systems, as compared to the usual situation, is that these peaks may be asymmetric because of Stark shifts. Initially neither Stark shifts nor Stark splittings are present. The evolution of the gain spectrum for $t>0$ gives therefore information on these effects in addition to providing means to determine effective Rabi frequencies and decay constants.

A. Resonant pumping

Conservation of energy implies that at the Stark shifted resonance $\Delta_1'=0$, we have $\Delta_2'=-\Delta_3'$. Introducing these values of the detunings into Eqs. (7) and (8) we obtain for the Laplace transform $\sigma_{23}^1(s)$ of $\rho_{23}^1(t)$

$$\sigma_{23}^1(s)=\left[\frac{iV_{23}|V_{21}|^2(s+\gamma_3)}{sD_{21}(s)D_{23}(s)}\right]\times\left[2\left[1-\frac{\gamma_2}{s+\gamma_3}\right](s+\gamma_{13}+i\Delta_2')+(s+\gamma_2)\right]\ , \tag{9}$$

where

$$D_{21}(s)=(s+\gamma_2)(s+\gamma_3)(s+\gamma_{21})+2|V_{21}|^2[2(s+\gamma_3)+\gamma_2]\ , \tag{10a}$$

$$D_{23}(s)=(s+\gamma_{23}+i\Delta_2')(s+\gamma_{13}+i\Delta_2')+|V_{21}|^2\ . \tag{10b}$$

The roots of the polynomials $D_{21}(s)$ and $D_{23}(s)$ determine the transient behavior of the probe gain, the pole $s=0$ being responsible for the steady state of the system. The three roots of $D_{21}(s)$ can be found approximately by applying the condition $\gamma_3 \gg \gamma_2$. In order to proceed, we rewrite $D_{21}(s)$ as

$$D_{21}(s)=(s+\gamma_3)[(s+\gamma_2)(s+\gamma_{21})+4|V_{21}|^2]+2|V_{21}|^2\gamma_2 \tag{11}$$

and solve perturbatively in the last term by using Newton's expansion technique.[18] The six poles of the Laplace transform Eq. (9) are then approximately given by

$$
\begin{aligned}
s_1 &= 0 , \\
s_2 &= -\gamma_3-(\gamma_2/2)A , \\
s_{3,4} &= -(\gamma_2+\gamma_{21})/2+\gamma_2 A/4 \\
&\quad \pm i[4|V_{21}|^2-(\gamma_2-\gamma_{21})^2/4 \\
&\quad +(\gamma_2 A/4)(2\gamma_3-\gamma_2-\gamma_{21})]^{1/2} , \\
s_{5,6} &= -(\gamma_{13}+\gamma_{23})/2-i\Delta_2' \\
&\quad \pm(i/2)[4|V_{21}|^2-(\gamma_{23}-\gamma_{13})^2]^{1/2} ,
\end{aligned}
\tag{12}
$$

where

$$
A=\frac{4|V_{21}|^2}{4|V_{21}|^2+(\gamma_2-\gamma_3)(\gamma_{21}-\gamma_3)} .
$$

The probe gain profile is proportional to the imaginary part of the inverse Laplace transform of $\sigma_{23}^1(s)$, which in turn has the form

$$
\rho_{23}^1(t)=\sum_i R_i \exp(s_i t) , \tag{13}
$$

where R_i is the residue corresponding to the pole s_i.

Let us briefly discuss each contribution in Eq. (13) to $\rho_{23}^1(t)$. (a) The steady-state term ($s_1=0$) consists of two peaks centered at $\Delta_2=\pm|V_{21}|$, in agreement with Ref. 15. (b) The s_2 contribution also exhibits two peaks centered at $\Delta_2=\pm|V_{21}|$, but it is negative and decays very rapidly at the rate γ_3. (c) The roots s_3 and s_4 can give rise either to pure exponential decay or to damped oscillations, depending upon the relative magnitudes of $|V_{21}|$ and $|\gamma_2-\gamma_{21}|/4$. Two situations are of particular spectroscopic relevance. In the weak-field limit, $|V_{21}| \ll |\gamma_2-\gamma_{21}|/4$, the roots s_3 and s_4 lead to exponential decay at rates γ_2 and γ_{21}. This regime is therefore suited for measuring atomic decay rates, especially the dipole forbidden decay rate γ_{21}. In the opposite limit, $|V_{21}| \gg |\gamma_2-\gamma_{21}|/4$, s_3 and s_4 give rise to a transient signal which decays at the approximate rate $(\gamma_2+\gamma_{21})/2$, and oscillates at approximately twice the effective two-photon Rabi frequency $2|V_{21}|$. This limit thus gives information on the two-photon matrix elements of the system. (d) Depending upon the relative magnitudes of $|V_{21}|$ and $|\gamma_{23}-\gamma_{13}|/4$, the square root in Eq. (12) yields either pure exponential decay or oscillations in the contributions due to s_5 and s_6. In the weak field regime $|V_{21}| \ll |\gamma_{23}-\gamma_{13}|/2$, the signals decay at rates γ_{23} and γ_{13} and oscillate at the beat frequency Δ_2'. (Recall that Δ_2' contains the ac Stark shifts.) For strong pump field, they decay at the average relaxation rate $(\gamma_{23}+\gamma_{13})/2$ and oscillate at the approximate superposition frequency $\Delta_2' \pm |V_{21}|$. For a long-lived upper state ($\gamma_3 \gg \gamma_2$) the s_5 and s_6 contributions decay away much faster than those due to s_3 and s_4, which, therefore, are responsible for the major features of the asymptotic transient behavior.

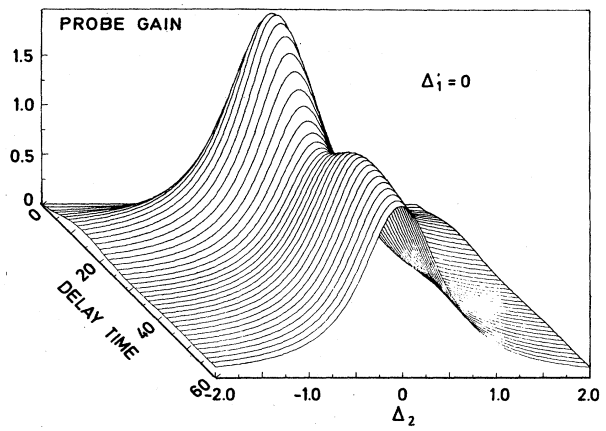

FIG. 2. Optical nutation signal for weak pump fields tuned to the Stark-shifted resonance $\Delta_1'=0$. The relaxation rates are $\gamma_2=0.03$, $\gamma_3=0.77$, $\gamma_{21}=0.1$, $\gamma_{23}=0.5$, and $\gamma_{13}=0.49$. The pump field intensity is such that $|V_{21}|=0.1<|\gamma_{21}-\gamma_2|/4$. All rates in nsec^{-1}.

In Fig. 2, we show the probe gain profile as a function of the delay time in a three-dimensional plot for a weak pump field, $|V_{21}| \ll |\gamma_2-\gamma_{21}|/4$ [see point (c) above]. Neither oscillations (those introduced by s_5 and s_6 are short lived and of small magnitude) nor any trace of Stark splitting is visible in the spectra. The transient consists of a superposition of two signals: the first, due to the two-photon coherence ρ_{21}, reaches its maximum rapidly and decays at the two-photon relaxation rate γ_{21}, while the second, essentially a population type contribution, reaches its maximum later and decays at the population rate γ_2 towards the steady-state value.

In Fig. 3(a), we show the time dependence of the probe gain $\rho_{23}(t)$ for a case where the two-photon Rabi oscillations dominate over the atomic decays. Figure 3(b) gives the corresponding contour plot. For short delay times, there is no visible signature of Stark splitting. It builds up only in times of the order of the inverse relaxation rates. Once the splitting is established, the gain profile mainly reflects the features of the $s_{3,4}$ contributions as discussed under (c). Figure 3(b) also shows that for some range of time delays, the Stark splitting is clearly better resolvable than in steady state. Such features are well-known in high-resolution spectroscopy and have been used in other contexts to achieve subnatural spectroscopy.[19]

B. Strong-field limit

As a second example, we consider the limit of small decay constants, especially the case where the phase relaxation rate γ_{21} of the ρ_{21} coherence is much smaller than the Rabi frequency V_{21}. In the general case $\Delta_1' \neq 0$, the Laplace transform $\sigma_{23}^1(s)$ of the matrix element $\rho_{23}^1(t)$ is

$$
\sigma_{23}^1(s)=\frac{iV_{23}|V_{21}|^2(s+\gamma_3)}{sD_{21}(s)D_{23}(s)}\left[2\left[1-\frac{\gamma_2}{s+\gamma_3}\right](s+\gamma_{13}-i\Delta_3')(s+\gamma_{21})+(s+\gamma_2)(s+\gamma_{21}+i\Delta_1')\right] , \tag{14}
$$

where $D_{21}(s)$ and $D_{23}(s)$ are the fourth- and second-order polynomials

$$D_{21}(s)=(s+\gamma_3)\left[(s+\gamma_2)[(s+\gamma_{21})^2+\Delta_1'^2]+2\,|\,V_{21}\,|^2\left[2+\frac{\gamma_2}{s+\gamma_3}\right](s+\gamma_{21})\right] \tag{15a}$$

and

$$D_{23}(s)=(s+\gamma_{23}+i\Delta_2')(s+\gamma_{13}-i\Delta_3')+\,|\,V_{21}\,|^2\,. \tag{15b}$$

The Laplace transform $\sigma_{23}^1(s)$ has therefore seven poles. Similarly to (11), approximate expressions for the poles may be obtained by reexpressing $D_{21}(s)$ as

$$D_{21}(s)=(s+\gamma_3)\left[(s+\gamma_2)[(s+\gamma_{21})^2+\Delta_1'^2+4\,|\,V_{21}\,|^2]+4\left[\gamma_{21}-\frac{\gamma_2}{2}\right]|\,V_{21}\,|^2\right]+2\,|\,V_{21}\,|^2\gamma_2(\gamma_{21}-\gamma_3) \tag{16}$$

and assuming the last term to be small, so that it can be treated as a small perturbation. This approximation is again based on our assumption of a long-lived upper state. The expressions for the poles s_i obtained from this analysis are quite complicated,[16] and we do not reproduce them here. Rather, we directly discuss the numerical examples of the strong-field regime.

Figure 4(a) shows the time-dependent gain spectrum for the case $\Delta_1=0$, $\Delta_1'=\omega_{s1}I_1=7.74$ nsec^{-1}, so that the effective detuning Δ_1' is due only to the Stark shift. The corresponding contour plot is shown in Fig. 4(b). For long delay times, i.e., as the system approaches steady state, it consists of two lines: one at the unshifted line center resonance $\Delta_2=0$, and the other at the Raman resonance $\Delta_2=\Delta_1'$, where the detuning is due to the power shift. (For a more detailed analysis, see Ref. 15.) The two peaks become resolved after a time about the inverse of the average relaxation rate $(\gamma_{13}+\gamma_{23})/2$. From there on, the population line approaches its steady-state value from below and the Raman line from above. The temporal oscillations occur at the frequency $(4\,|\,V_{21}\,|^2+\Delta_1'^2)^{1/2}$. The short-time behavior is characterized by a broad, single-

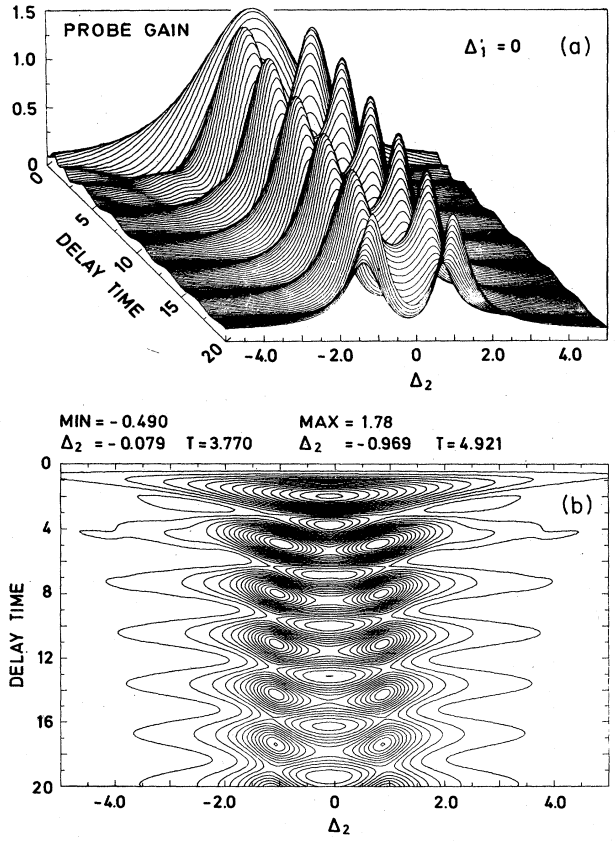

FIG. 3. (a) Transient probe gain following the switch on of a pump field with $|\,V_{21}\,|=1>|\gamma_{21}-\gamma_2|$ and tuned to the Stark-shifted resonance $\Delta_1'=0$. Relaxation rates as in Fig. 2. (b) Corresponding contour plot.

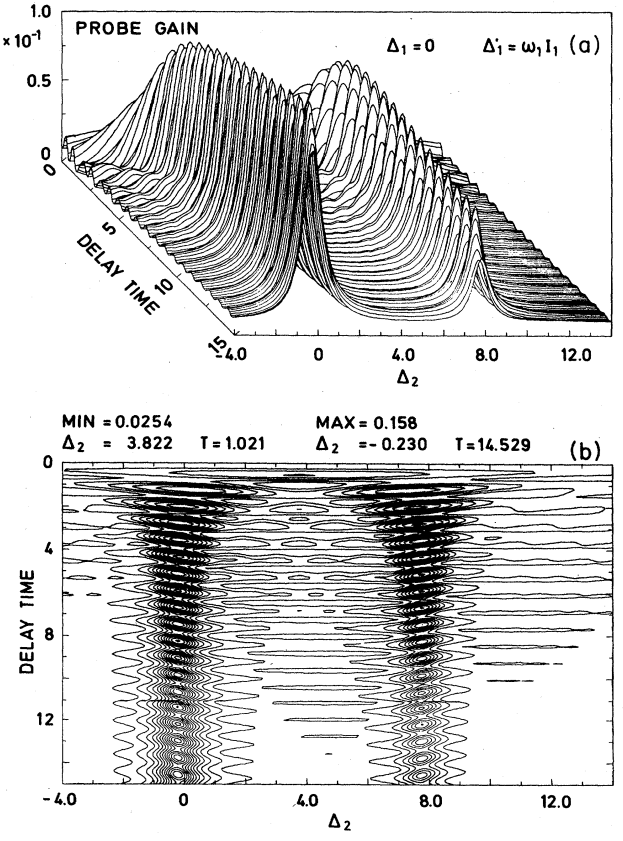

FIG. 4. (a) Transient probe gain under excitation at the Stark-shifted resonance $\Delta_1=0$. In this case, the pump detuning $\Delta_1'=7.74$ nsec^{-1} is caused by Stark shifts. (b) Corresponding contour plot. Relaxation rates as in Fig. 2.

peaked gain curve centered about halfway between the two steady-state resonances [see the contour plot, Fig. 4(b)].

The plots correspond to the case $\gamma_{21} < \gamma_{23}, \gamma_{13}$, in accordance with the assumption $\gamma_2 \ll \gamma_3$. All relaxation rates are small compared to the effective two-photon Rabi frequency, in which case the probe gain allows to determine both the effective two-photon Rabi frequency and the Stark shifts of the system. The observation of the optical nutation may also be an efficient means to determine experimentally the position of the Stark-shifted resonance. The minimum oscillation frequency of the transient signal occurs when the pump detuning cancels the Stark shifts, and equals then approximately twice the effective two-photon Rabi frequency.

IV. FREE-INDUCTION DECAY

For square pump pulses long compared to the inverse relaxation rates of the system, the steady state is reached before the pump falls off. Thereafter, the steady-state populations and coherences evolve "freely," except for the interaction with the probe field E_2 which remains applied to the system. The free pump field solution is obtained from Eqs. (7) and (8) by setting $V_{21}=0$. The probe gain is then proportional to the imaginary part of

$$\rho_{23}^{1}(t)=\rho_{23}(t_0)e^{-(\gamma_{23}+i\Delta_2)(t-t_0)}+iV_{23}\rho_{22}(t_0)\left[\frac{\gamma_3-2\gamma_2}{\gamma_3-\gamma_2}\right]\left[\frac{e^{-\gamma_2(t-t_0)}-e^{-(\gamma_{23}+i\Delta_2)(t-t_0)}}{\gamma_{23}+i\Delta_2-\gamma_2}\right]$$
$$-iV_{23}\left[\rho_{33}(t_0)-\left[\frac{\gamma_2}{\gamma_3-\gamma_2}\right]\rho_{22}(t_0)\right]\left[\frac{e^{-\gamma_3(t-t_0)}-e^{-(\gamma_{23}+i\Delta_2)(t-t_0)}}{\gamma_{23}+i\Delta_2-\gamma_3}\right]. \quad (17)$$

This expression contains three contributions: the standard free-induction decay of the coherence $\rho_{23}(t_0)$ at the rate γ_{23}, and the couplings of the initial populations $\rho_{22}(t_0)$ and $\rho_{33}(t_0)$ with the probe field.

Figure 5(a) shows the free decay of the initial polarization $\rho_{23}(t_0)$ at the Stark-shifted two-photon resonance ($\Delta_1'=0$) after steady-state preparation, i.e., $\rho_{22}(t_0)$, $\rho_{33}(t_0)$, and $\rho_{23}(t_0)$ are chosen as the steady-state solutions of Eqs.

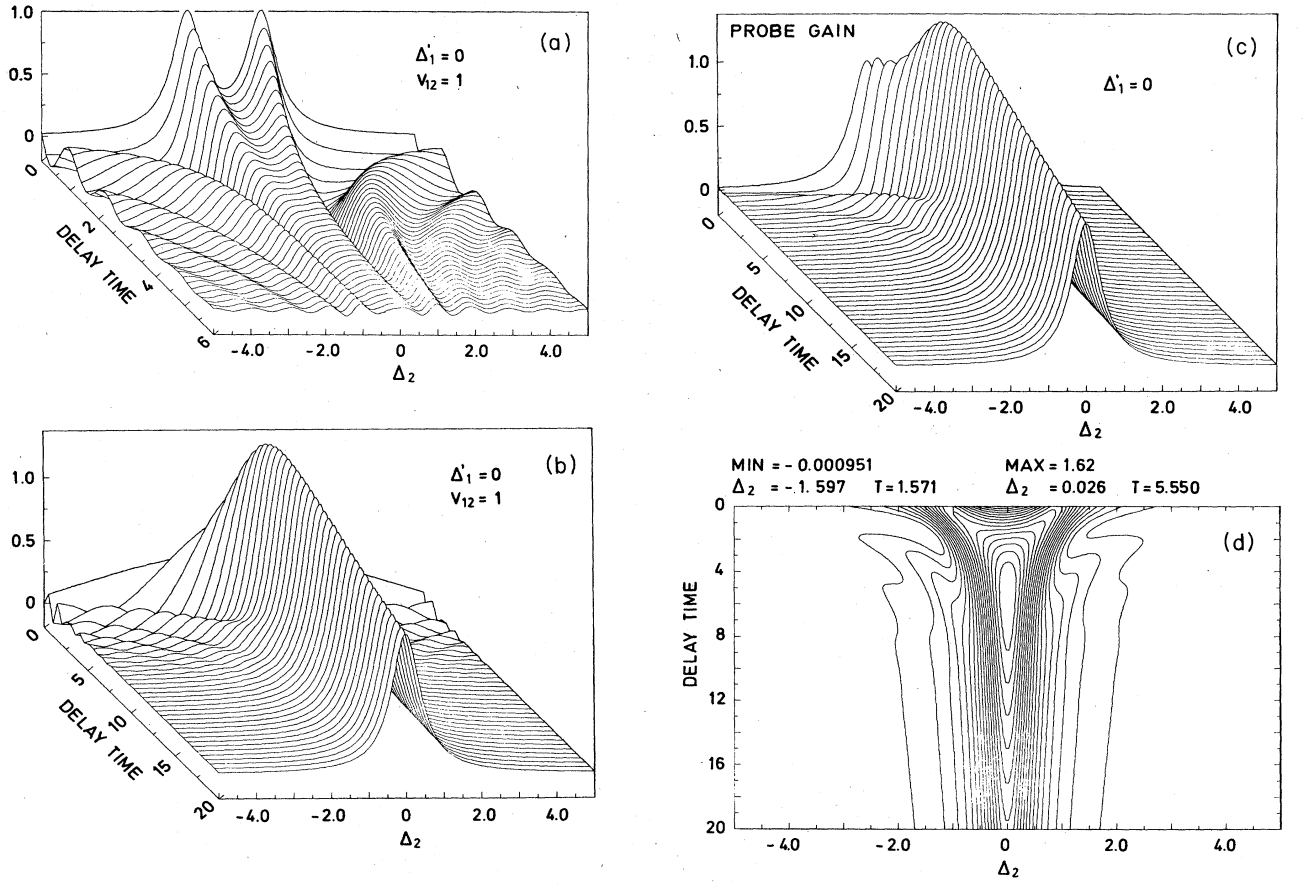

FIG. 5. Free-induction decay following pumping at the Stark-shifted resonance $\Delta_1'=0$. $V_{21}(t<t_0)=1$ nsec^{-1}, and relaxation rates as in Fig. 2. (a) Free decay of the coherence $\rho_{23}(t_0)$ [first term in Eq. (17)]; (b) contribution of the population term $\rho_{22}(t_0)$ [second term in Eq. (17)]; (c) total free-induction signal; (d) corresponding contour plot.

(7) and (8). An interesting feature is the oscillatory decay of the Stark splitting due to $\Delta_2 \neq 0$.

The contribution of the population term $\rho_{22}(t_0)$ in the second term of Eq. (17) is illustrated in Fig. 5(b). At $t=t_0$ it is zero, then starts growing around $\Delta_2=0$, reaching a maximum at a delay time

$$T=t-t_0=\frac{\ln(\gamma_{23}/\gamma_2)}{\gamma_{23}-\gamma_2} . \tag{18}$$

Thereafter it decreases at the population decay rate γ_2.

The contribution of the last term in Eq. (17) is of the order of γ_2/γ_3 smaller than the second term, and is therefore negligible in our limit of the long-lived upper level. The total gain spectrum is plotted in Fig. 5(c). Because of $\gamma_3 \gg \gamma_2$, we have $\gamma_{23} > (\gamma_2+\gamma_3)/2 > \gamma_2$, implying that the long-time behavior is determined by the $\rho_{22}(t_0)$ contribution, whereas for short delay times, the free decay of $\rho_{23}(t_0)$ dominates. The contour plot Fig. 5(d) further illustrates the relaxation of the Stark split spectrum to a Lorentzian. The maximum of the total gain spectrum is approximately reached after the delay time given by Eq. (18).

Figure 6 shows the gain spectrum when pumping at $\Delta_1=0$, i.e., $\Delta_1'=\omega_{s1}I_1$. After reaching a maximum, the population signal decays at the rate γ_2, while the Raman line, centered at $\Delta_2=\Delta_1'$, relaxes as the ρ_{23} coherence at the assumedly much faster relaxation rate γ_{23}. If the probe were absent, no gain signal would be present at the atomic frequency. Through the interaction with the probe field, we have now the additional possibility of collecting information about the upper-state population and its relaxation rate.

V. GAUSSIAN PUMP PULSES

We now turn to the more realistic case of Gaussian pump pulses, for which new effects can appear because of the time-dependent Rabi frequency, and also because of the temporal sweeping of the ac Stark shifts. We have solved Eqs. (2) numerically in this case, and will discuss some examples for two different regimes: the strong pump limit, where the maximum Rabi frequency is larger than the relaxation rates and rapid transients dominate, and the opposite case where the coherence relaxation rates are larger than the Rabi frequency and the polarizations are able to follow adiabatically the field variations.

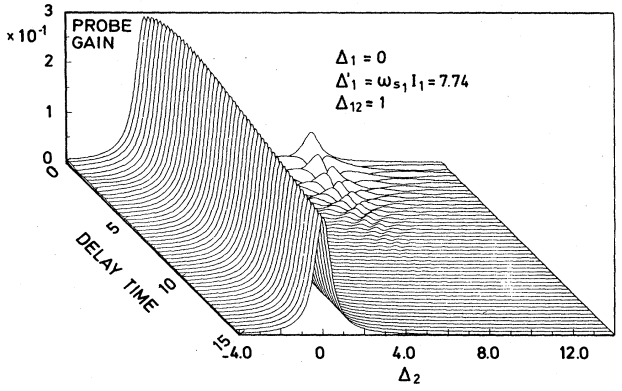

FIG. 6. Gain spectrum following pumping at the two-photon resonance $\Delta_1=0$. The uncompensated Stark shift equals $\Delta_1'=7.74$ nsec^{-1}. Relaxation rates as in Fig. 2.

A. Strong pump field

We consider first the case where all decay rates are small compared to the maximum effective two-photon Rabi frequency $V_0=|V_{21}^{\max}|$. The probe field is taken to be constant, and the corresponding Rabi frequency $|V_{23}|$ much smaller than V_0. Figure 7 shows gain profiles for (a) resonant and (b) detuned pumping, with the corresponding contour plots. Here, the ac Stark shifts have been arbitrarily set equal to zero. This simplification allows to distinguish effects due to sweeping of the two-photon pumping rates from those due to the ac Stark shift modulation.

At resonance, the maximum gain appears at the atomic frequency ω_{23} ($\Delta_2=0$) and occurs after the pulse is over ($t=16.67$ nsec). This maximum is closely related to the population transient of free-induction decay found in Sec. IV. The gain maximum has a long tail decaying at the rate γ_2. During the pump pulse, the gain spectrum is reminiscent of the optical nutation signal. We observe Rabi oscillations as well as the buildup of a Stark splitting.

As an example of detuned pumping, we show in Fig. 7(b) the probe gain profile for $\Delta_1=8$ nsec^{-1}, with its corresponding contour plot. The Raman gain, centered at $\Delta_2=\Delta_1$, and the population line centered at $\Delta_2=0$, are well separated in the time-frequency plane. The Raman gain is larger than the population signal by about a factor of 1.5. As expected, it exists only during the pump pulse, in contrast to the gain at the atomic frequency, which persists and reaches its maximum after the pump pulse is over, around $t=16$ nsec. This behavior is related to the free-induction decay and off-wing pumping of population to level $|2\rangle$.

When Stark shifts are included, the gain spectra become more complicated. In Fig. 8 we show results obtained for (a) resonant and (b) detuned pumping. The maximum ac Stark shift is chosen as $\omega_{s1}I_1^{\max}=7.74$ nsec^{-1}. At the unshifted two-photon resonance ($\Delta_1=0$ and $\Delta_1'=\omega_{s1}I_1$), we observe a strongly oscillating signal during the pump pulse, as well as a population signal centered around $\Delta_2=0$ reaching its maximum after the pump pulse. The rapidly varying signals are hard to analyze and would probably be smeared away in experiments. The population signal resembles that of Fig. 7(b). This is expected, since the population contribution depends mainly on the population of the upper state at the end of the pulse.

The signal behavior can be understood as follows: at the leading edge of the pulse, the intensity is too small to considerably shift the levels. The gain spectrum has a single maximum near $\Delta_2=0$. As time elapses, the pump intensity increases and the levels are pushed away, with the appearance of a Raman signal around $\Delta_2=\Delta_1'$. Contrary to the case of Fig. 7(b), the Raman signal remains smaller than the population contribution at the end of the pulse. This is not surprising. By setting the Stark shifts equal to

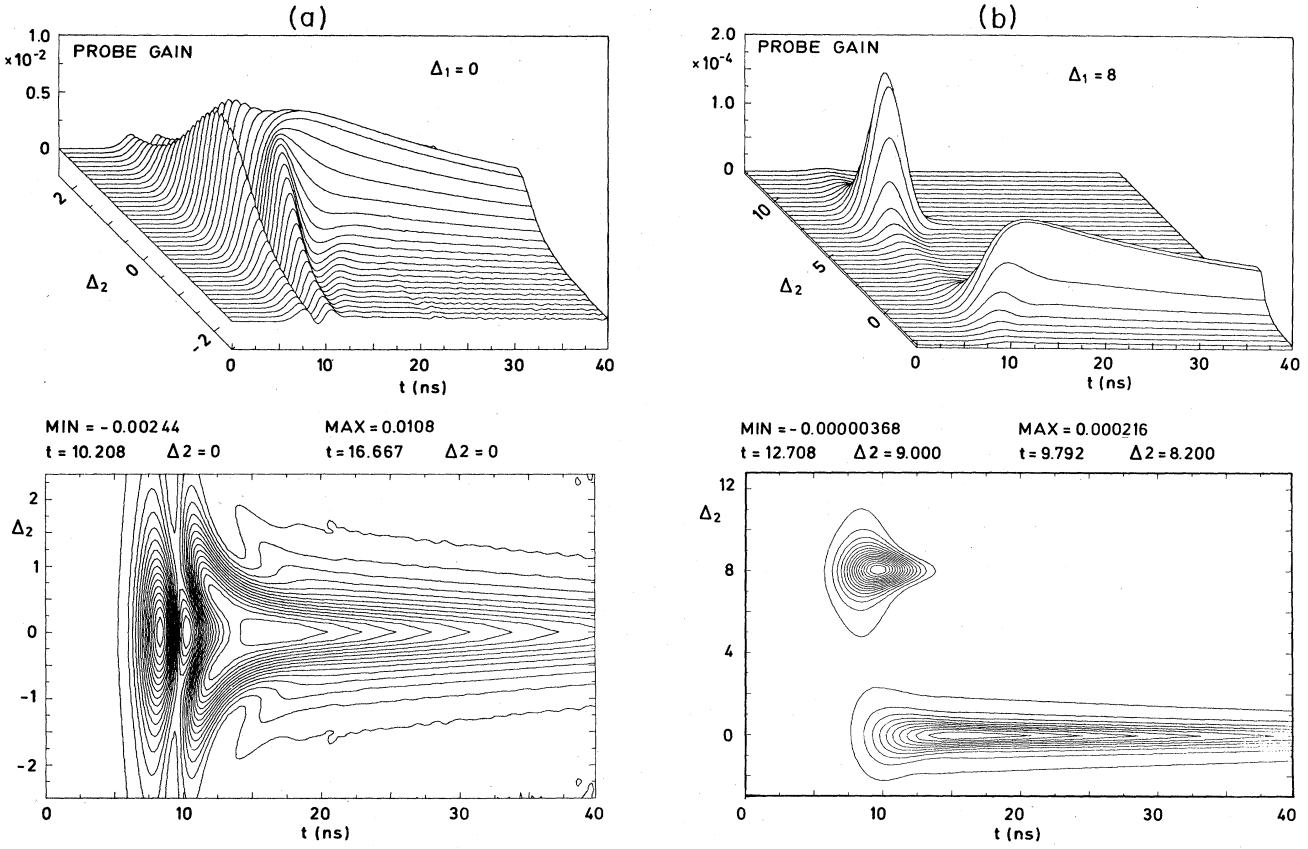

FIG. 7. (a) Probe gain spectrum under pumping at the two-photon resonance $\Delta_1=0$ as a function of time and probe detuning, with corresponding contour plot. Here, the Stark shifts have been arbitrarily set to zero. The relaxation rates are $\gamma_2=0.03$, $\gamma_3=0.77$, $\gamma_{21}=0.1$, $\gamma_{23}=0.5$, and $\gamma_{13}=0.49$, and $V_{21}^{\max}=1$, all in units of nsec^{-1}. The pump pulse is a Gaussian of 6 nsec width peaking at $t=9$ nsec. (b) Probe gain and corresponding contour plot for detuned pumping ($\Delta_1=8$ nsec^{-1}). All other constants as in (a).

zero, one keeps the atomic levels fixed so that the pump detuning is constant. In reality, however, the pump of course pushes the levels away and back producing a time-dependent detuning which varies from zero to $\omega_{s2}I_1^{\max}$.

Figure 8(b) shows the gain spectrum as a function of time when a finite pump detuning is present in addition to the Stark shift. Its structure is clearly closer to that of Fig. 7(b). The Raman line with maximum around $\Delta_2=\Delta_1'$ can clearly be distinguished from the population line at $\Delta_2=0$. This is because in this case, the maximum Stark shift does not anymore dominate over the fixed detuning Δ_1. Indeed, as would be expected, as the fixed detuning is further increased, the role of the time-dependent Stark shift becomes less important, and can be neglected for $\Delta_1 \gg \omega_{s1}I_1$.

B. Fast decay rates

As already mentioned, when the decay rates are much larger than the maximum Rabi frequency and the inverse of the pulse duration, the transients are effectively damped out. In Fig. 9 we show the Stokes gain for transversal decay rates much larger than the two-photon effective Rabi frequency. The Gaussian pump pulse is also shown in dashed line. The Stokes gain does not exhibit oscillations any longer, as the system has now time to reach steady-state values during the pump pulse: the off-diagonal density matrix element ρ_{21} follows adiabatically the pump. Even the gain growth after the pulse due to the population term ρ_{22} becomes less spectacular here, because the delay time needed to reach its maximum is now very short [see Eq. (18)]. The gain maximum turns out to be quite close to the corresponding calculated steady-state value. Only the long tail decaying at rate γ_2 reminds us of the transient character of the population signal.

VI. DISCUSSION

Our study of two-photon—pumped three-level systems opens up new possibilities to measure Rabi frequencies and decay rates, especially those connected with the two-photon coherence between states of same parity. The time-frequency method employed here provides a way to follow the onset of Stark shifts and splittings.

In order to simplify the analytical work, the assumption $\gamma_2<\gamma_{21}<\gamma_{23},\gamma_{13}$ was made. In this case, we found that Raman-type processes have their maximum in the optical

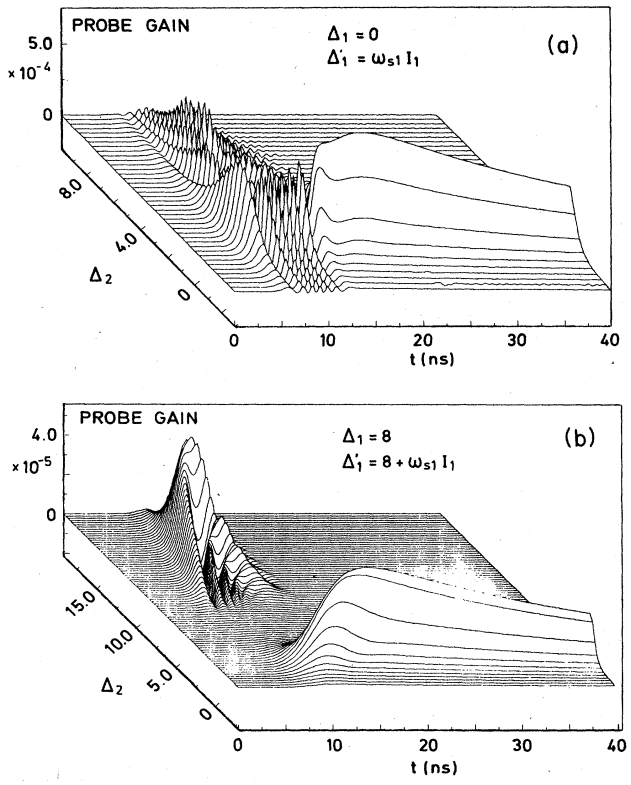

FIG. 8. Probe gain spectrum when Stark shifts are included, i.e., $\omega_{s1} I_1^{max} = 7.74$ nsec^{-1}. (a) $\Delta_1 = 0$; (b) $\Delta_1 = 8$. Other parameters as in Fig. 7.

nutation regime and quickly die out as the pump field is switched off. The "free-induction decay" regime is dominated by the presence of a population-type line.

Further relevant features found are the following: (a) The buildup of Stark splittings occurs in times of the order of the inverse coherence relaxation rate of the intermediate level; (b) the resolution of the Stark splittings obtainable in the optical nutation regime is better than in the steady state; and (c) the highest Raman and population signals are obtained during the transients—the first in the optical nutation, and the second in the free-induction regime.

The study of the probe gain for Gaussian pump pulses

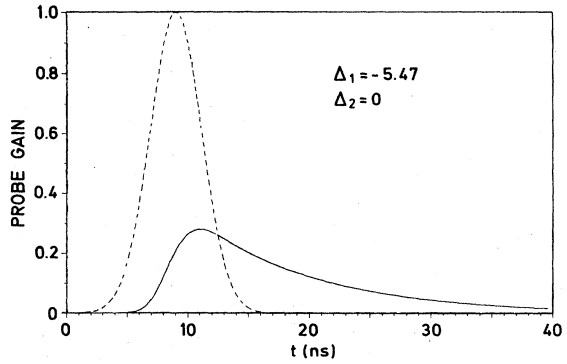

FIG. 9. Temporal shape of the probe gain for fast relaxation rates. The Stark shifts have been included, and $\gamma_2 = 0.1$, $\gamma_3 = 1$, $\gamma_{21} = \gamma_{23} = \gamma_{13} = 10$ (in nsec^{-1}). The pump pulse (dashed line) is the same as in Fig. 7.

yields additional, more realistic information which can be applied, e.g., in analyses of the dynamics of optically pumped lasers. For resonant pumping and in the case of slow decay constants, both the optical nutation and the population transient in the free-induction decay regime contribute to the probe gain. A clear temporal distinction between population-type and Raman-type lines is seen for large pump detunings. While the Raman line exists only during the pump pulse, a strong population line with a long tail due to the slow population decay appears after the pump pulse is over.

Finally, we point out that the study of transients for Gaussian pump pulses leads to results complementary to those obtained in steady state,[15] which do not provide the full picture. In particular, while the steady-state gain is maximum at the atomic frequency even for off-resonant pumping, in the case of a Gaussian pump the Raman line gain can be maximum at the leading edge of the pulse. This is a consequence of optical nutation in the case of relaxation rates small compared with the Rabi frequency.

ACKNOWLEDGMENTS

A.G.G. acknowledges support from Deutscher Akademischer Austauschdienst (Bonn, Germany) and Universidad Nacional de Colombia. The work of R.R.E.S. was partly performed while on sabbatical leave at the Max-Planck-Institut für Quantenoptik.

[1]M. Ducloy, Y. Leite, and M. S. Feld, Phys. Rev. A **17**, 623 (1978).
[2]R. G. Brewer and E. L. Hahn, Phys. Rev. A **11**, 1641 (1975).
[3]P. R. Berman and R. Salomaa, Phys. Rev. A **25**, 2667 (1982).
[4]D. Grischkowsky, M. M. Loy, and P. F. Liao, Phys. Rev. A **12**, 251 (1975).
[5]B. Hocker and C. L. Tang, Phys. Rev. **184**, 356 (1969); R. G. Brewer and R. L. Shoemaker, Phys. Rev. Lett. **27**, 631 (1971).
[6]A. Schenzle and R. G. Brewer, Phys. Rev. A **14**, 1756 (1976); Phys. Rep. **43**, 455 (1978).
[7]R. L. Shoemaker and R. G. Brewer, Phys. Rev. Lett. **28**, 1430 (1972).
[8]R. G. Brewer and R. L. Shoemaker, Phys. Rev. A **6**, 2001 (1972).
[9]N. A. Kurnit, I. D. Abella, and S. R. Hartmann, Phys. Rev. Lett. **13**, 567 (1964); C. K. N. Patel and R. E. Slusher, *ibid.* **20**, 1089 (1968).
[10]T. W. Mossberg, R. Kachru, S. R. Hartmann, and A. M. Flusberg, Phys. Rev. A **20**, 1976 (1979).
[11]N. Tan-no, K. Yokoto, and H. Inaba, Phys. Rev. Lett. **29**,

1211 (1972).
[12]M. S. Feld, in *Frontiers in Laser Spectroscopy,* edited by R. Balian, S. Haroche, and S. Liberman (North-Holland, Amsterdam, 1976).
[13]M. Goppert-Mayer, Ann. Phys. (Leipzig) **9**, 273 (1931).
[14]M. Takatsuji, Phys. Rev. A **11**, 619 (1975).
[15]A. Guzman de Garcia, P. Meystre, and M. Sargent III, Opt. Commun. **43**, 364 (1982).
[16]A. Guzman de Garcia, Ph.D. thesis, Ludwig-Maximilian University, Munich, 1984.
[17]H. G. von Garssen, private communication. This author has developed a computer code that determines systematically all frequency combinations necessary to properly describe the evolution of the atomic density matrix.
[18]F. S. Acton, *Numerical Methods that Work* (Harper and Row, New York, 1970).
[19]D. O'Brien, P. Meystre, and H. Walther, in *Advances in Atomic and Molecular Physics* (Academic, New York, 1985), pp. 1—49.